CRYSTAL Research & Technology

Cryst. Res. Technol. 49, No. 11, 850–859 (2014) / DOI 10.1002/crat.201400174

Original Paper

A method to model the transient performance of high frequency vibration in crystal growth

XiaoLong Li[1], *YunZhong Zhu*[2], *YuLan Liu*[1,*], *and Biao Wang*[2,*]

Received 27 May 2014, revised 2 October 2014, accepted 8 October 2014
Published online 6 November 2014

A general method to quantitatively study the transient fluctuation related to the high frequency vibration in crystal growth is developed. An example during the Czochralski crystal growth has been simulated, and the simulation coincides with the experimental date. On basis of the model, the influence of vibration frequency on the transient fluctuations for temperature and velocity are elucidated. Then an available approach to control the vibration effect is proposed.

1 Introduction

Vibration is a built-in phenomenon in the crystal growth system. Both the vibration caused by the induced heating device and artificial vibration will give rise to the transient fluctuation of crystal growth environment [1–7]. Studying and controlling the vibration in crystal growth are a promising approach to improve the crystal performance. Extensive experiments are carried out to investigate the influence of the vibration on crystal growth [8–15]. Numerical simulation has also been used to investigate the effect of vibration on the melt convection [16, 17]. However, most of the melt has a thermal diffusivity less than 10^{-5} m^2/s, as well as the momentum diffusivity [18]. The relaxation time related to temperature and velocity is about 10 s in a 10 cm-diameter container. To recognize a vibration of 1 kHz, the time step for numerical simulation is, at least, 10^{-4} s. The relaxation time for diffusion is about 10^5 orders of magnitude larger than the time step for vibration. Both the built-in vibration due to the induced heating system and the artificial vibration may have a higher frequency, and the time step is shorter. It is impossible for numerical simulation to recognize so fast vibration and so slow diffusion process simultaneously. This is the major restrictive factor on using numerical simulation to investigate the vibration effects in crystal growth systems.

It is our purpose in this paper to address this problem. Firstly, the simulation method is derived carefully. Secondly, the model we solved is described in detail. The governing equations and the boundary conditions are formulated. Thirdly, the simulation is described step by step. At last, we will explain the simulation result and compare it with the experiment. The influences of vibration frequency on the transient fluctuations of temperature and velocity are analyzed. Then an available approach to control the vibration effect is proposed.

2 Methodology and model

2.1 Methodology

We choose the CZ crystal growth configuration to illustrate our method, because we have the CZ experiment device. The simulation results can be compared with the experiment. The experimental device is represented in figure 1(a). For simplicity and clarity, our description is carried out on the basis of the crucible vibration caused by the high frequency electromagnetic field in the CZ configuration. It can be easily extended to other situations. A simple schematic diagram of CZ crystal growth configuration is shown in figure 1(b). The cylindrical melt geometry is presented individually in figure 1(c). The height is 16 mm, the radius of the melt and the solid-liquid interface are 35 mm and 15 mm, respectively. As shown in figure 1(c), the crucible vibrates as

* Corresponding authors: e-mail: stslyl@mail.sysu.edu.cn, wangbiao@mail.sysu.edu.cn
[1] School of Engineering, Sun Yat-sen University, Guangzhou, 510275, China
[2] School of Physics and Engineering, Sun Yat-sen University, Guangzhou, 510275, China

CRYSTAL Research & Technology

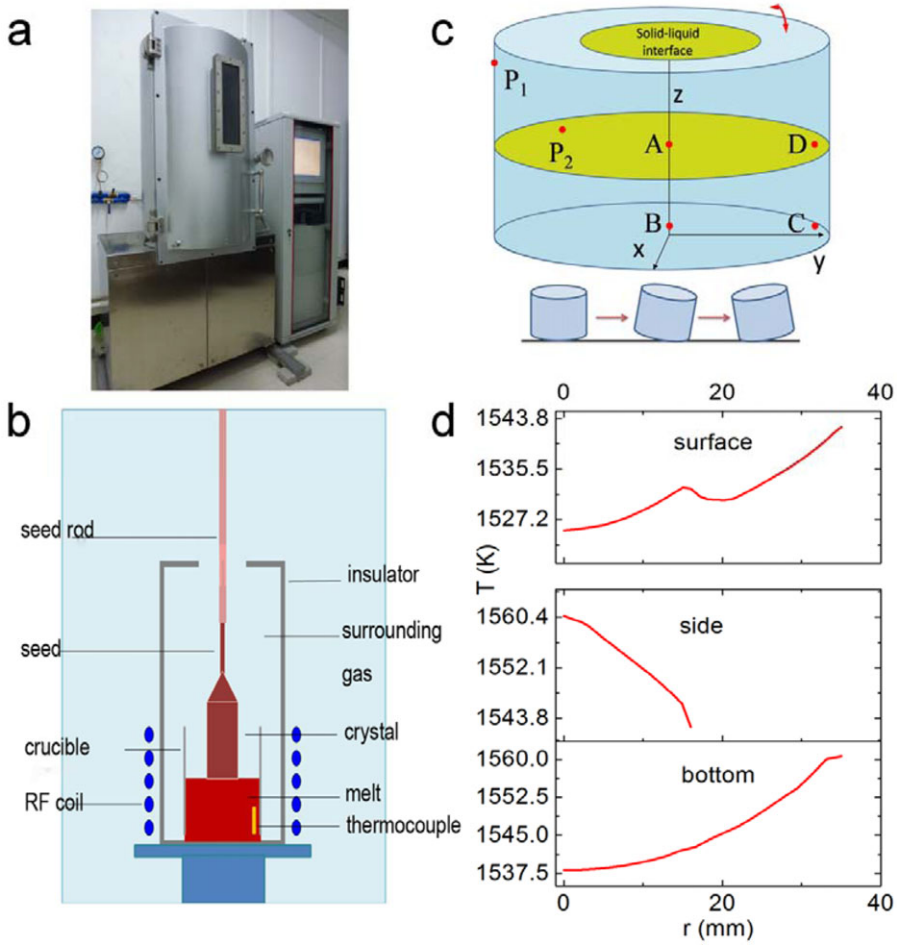

Fig. 1 (a) Experimental device; (b) Schematic diagram of CZ crystal growth configuration; (c) The model geometry used for 3D simulation, points A, B, C and D are the reference points. The solid-liquid interface and the cross section are marked with low yellow color. The red arrow and three cylinders at the bottom indicate the vibration direction; (d) the thermal boundary conditions.

an entirety, just like a tumbler. The vibration is periodic and non-axisymmetric. The red arrow and three cylinders at the bottom indicate the vibration direction. When the vibration generates at the crucible wall (represented by point P_1), it will propagate in the melt and cause velocity and temperature fluctuations throughout the melt (P_2 is marked as the representative point). If the fluctuation generates at the moment t_2 at the point P_2, which is caused by the vibration of the point P_1 at the moment t_1, is denoted by $f(P_1, t_1, P_2, t_2)$. The realistic fluctuation generates at the moment t_2 at point P_2 due to the collective vibration of the whole crucible wall at the moment t_1, can be written as follow,

$$F(P_2, t_2) = \int_S \left[\int_0^{t_2} \nu f(P_1, t_1, P_2, t_2) dt_1 \right] dP_1 \quad (1)$$

Herein, S is the total area of the crucible wall, and ν is the frequency of crucible vibration. νdt_1 means the crucible vibration times within the time interval dt_1, $f(P_1, t_1, P_2, t_2)$ means the fluctuation amplitude caused by the vibration of the point P_1. Thus, the term in the square brackets is the realistic fluctuation caused by the vibration of the point P_1. In addition, the expression $\nu f(P_1, t_1, P_2, t_2)$ can be explained as the fluctuation rate of the point P_2. The vibration energy will be dissipated by the viscosity dissipation of the melt, and by the boundary diffusion to the surrounding, so the vibration has a finite lifetime lifetime (denoted by τ). That is, the influence of the crucible vibration on the melt is limited within a certain time τ. Only the surviving vibration has an effect on the melt. Thus, Eq. (1) is written as

$$F(P_2, t_2) = \int_S \int_{t_2-\tau}^{t_2} \nu f(P_1, t_1, P_2, t_2) dt_1 dP_1 \quad (2)$$

Here, we introduce the conception of vibration mode to represent one stationary state of the system related

to the vibration at some part of the crucible wall at any moment. If the realistic fluctuation is considered as a collective effect of different vibration modes, all of the vibration modes, synchronously caused by the vibration of the whole crucible wall, can be considered as one vibration mode. Based on the above analysis, Eq. (2) can be reduced to

$$F(P_2, t_2) = \int_{t_2-\tau}^{t_2} v f(t_1, P_2, t_2) dt_1 \tag{3}$$

The vibration modes at different moments can be numerically simulated by use of a stationary method. Then according to Eq. (3), the transient fluctuations can be computed by adding the effects of the vibration modes related to different moments together. Up to now, a transient problem is converted to a stationary problem, and the vibration effects related to different parts of the crucible wall at different moments are completely coupled.

Although this method can completely couple the vibration effects, many times stationary computations are needed to get the transient fluctuation of one moment. As the time scale of the transient model increases, the computation frequency of the stationary model increases dramatically. Fortunately, in most cases, the vibration source is periodic or can be approximated as periodic vibration, thus the vibration mode is also periodic. Therefore, only the vibration modes during one vibration period are needed to get the transient fluctuations at any moment.

2.2 Model

As mentioned above, an example during the Czochralski(CZ) crystal growth is chosen to make the simulation comparable to the experiment. To obtain the vibration modes, a 3D simulation is carried out on basis of a self-developed CZ crystal growth furnace of $LiNbO_3$. Whereas, a global 3D simulation with the energy, momentum and radiation heat transfer involved is cumbersome and unnecessary. Only the cylindrical melt geometry is extracted as the model geometry, as shown in figure 1(c). The crystal growth rate is negligible compared to the vibration and fluctuation rates, so the model geometry is considered as invariable. The Boussinesq hypothesis is used to describe the gravity effect. The melt is incompressible and the flow is laminar. All of the property parameters are extracted from references [19, 20]. The governing equations are the energy and momentum conservation equations as follow [21],

$$\nabla.\mathbf{U} = 0 \tag{4}$$

$$\rho\mathbf{U}.\nabla\mathbf{U} = -\nabla P + \nabla.\underline{\tau} + \rho_0\mathbf{g}\beta(T - T_0) \tag{5}$$

$$\rho C_p T\nabla.\mathbf{U} = \lambda\nabla^2 T \tag{6}$$

$$\tau_{ij} = \mu\left(\frac{\partial u_i}{\partial x_j} + \frac{\partial u_j}{\partial x_i}\right) - \frac{2}{3}\mu\delta_{ij}\nabla.\mathbf{U} \tag{7}$$

Here, ρ is the density, ρ_0 is the reference density, $\mathbf{U}$ is the velocity vector, $\underline{\tau}$ is the stress tensor, Eq. (7) shows the components, $\mathbf{g}$ is the gravity vector, P is the pressure, μ is the dynamic viscosity, C_p is the specific heat, T is the temperature, λ is the thermal conductivity, and β is the thermal expansion coefficient.

The thermal boundary conditions are obtained from a global two-dimensional (2D) axisymmetric simulation. The 2D simulation is implemented on the CGSim platform (which is a professional software for numerical simulation of crystal growth). Figure 1(d) shows the temperature distributions from the 2D simulation at the surface, the side and the bottom of the model geometry. These results are in excellent agreement with the experimental results [22].

To integrate the vibration effects caused by the high frequency electromagnetic field, the crucible vibration is assumed to be periodic and has the same frequency as the electromagnetic field. The velocity boundary conditions at the bottom and the side of the model geometry are formulated as follow,

$$u = v = w = A\cos(2\pi\, par) \tag{8}$$

Where, u, v, w are the velocity components. A is the vibration velocity amplitude, and par is a variable parameter. Table 1 shows the parameter group in this work. According to the experiment traces on the crucible

Table 1 Parameter groups.

A (mm/s)	par (period)				
0.10	0.00	0.25	0.50	0.75	1.00
0.20	0.00	0.25	0.50	0.75	1.00
0.50	0.00	0.25	0.50	0.75	1.00
1.00	0.00	0.25	0.50	0.75	1.00

CRYSTAL Research & Technology

substrate, the maximal deviation of the crucible from the equilibrium position is about 0.5 mm. As shown in Table 1, A is set to be 0.10, 0.20, 0.50 and 1.00 mm/s. For each vibration velocity amplitude, *par* varies from 0 to 1 with an increment of 0.25, corresponds to a quarter of the vibration period.

At the solid-liquid interface, the crystal has a rotation rate of 15 rpm. The gas-melt interface yields a thermal Marangoni force [20], formulated as follow,

$$\sigma = \sigma_T \nabla T \tag{9}$$

Here, σ_T is the surface tension coefficient related to temperature.

3 The simulation steps

The computation is implemented by use of the finite-element-method software COMSOL MULTIPHYSICS. As displayed in figure 1(c), four points of A, B, C and D are chosen as the test points. Because the Dirichlet boundary conditions are used at the wall and at the interface (described in part 2), every coordinate is chosen 2 millimeters away from the boundary to decrease the effect of the boundary layer. The coordinates of these points are listed in Table 2.

3.1 The vibration modes

A cross section at the center of the cylinder is picked up to investigate the effects of the vibration source phase shift on the vibration mode, as shown in figure 1(c). The temperature fluctuation in the central cross section is shown in figure 2(a). As *par* varies from 0 to 0.5 (corresponding to the phase shift changes from 0 to π.), the large negative fluctuation in the up edge area shifts towards the down edge area. The large positive fluctuation at the down edge damps slowly and shifts slowly towards the up edge. And the negative fluctuation in the right edge area shifts towards the left edge area. It comes from the periodic variation of the vibration direction. The central part maintains a large negative fluctuation, which results from the coupling interaction of the surrounding fluctuation in the melt. To have an insight into the fluctuation modes, the velocity fluctuation is investigated and shown in figure 2(b). The positive fluctuation in the right edge area fades away, and the negative fluctuation arises in the left edge area. The central part maintains a large positive velocity fluctuation, which corresponds to a strengthening heat flux. This heat flux results in a large negative temperature fluctuation. For a boundary vibration velocity amplitude of 0.5 mm/s, the temperature fluctuation is $-18.5 \sim 17$ K, and velocity fluctuation is $-4.85 \sim 6.35$ mm/s.

Table 2 The coordinates of the reference points.

Reference point	x (mm)	y (mm)	z (mm)
A	0	0	8
B	0	0	2
C	0	33	2
D	0	33	8

3.2 Evaluate the transient performance

In order to get the transient performance of the fluctuation caused by crucible vibration, the vibration modes of temperature and velocity are investigated at the reference points. Figure 3 and figure 4 display the temperature and velocity fluctuations during one period, respectively. All of the fluctuation amplitudes increase as the vibration source amplitudes increase. During the early quarter and the late quarter of a period, the vibration mode has the same extreme of amplitude (denoted by A_1). In the middle stage, it has another extreme of amplitude (denoted by A_2). Because the vibration source (velocity boundary conditions) used in the simulation is a cosine function, we suppose the vibration mode in the melt is a cosine function too. The vibration mode has the same frequency as the vibration source. Then the vibration mode can be formulated as $A(t)\cos(2\pi\nu t)$.

$$A(t) = \begin{cases} A_1 & \frac{n}{\nu} \le t \le \frac{n}{\nu} + \frac{1}{4\nu} \quad or \quad \frac{n}{\nu} + \frac{3}{4\nu} \le t \le \frac{n+1}{\nu} \\ A_2 & \frac{n}{\nu} + \frac{1}{4\nu} \le t \le \frac{n}{\nu} + \frac{3}{4\nu} \end{cases} \tag{10}$$

Where, all A_1 and A_2 are obtained from the simulation, and $n$is a positive integer. Table 3 lists the value of A_1 and A_2 related to the temperature and Table 4 is related to the velocity.

To obtain the transient fluctuation performance, the lifetime of the vibration mode is estimated by the sound velocity in the melt. Since no reliable value of sound velocity is available to $LiNbO_3$ melt, the correlation derived from experiment data between surface tension, density, and sound velocity in liquid metals is used to

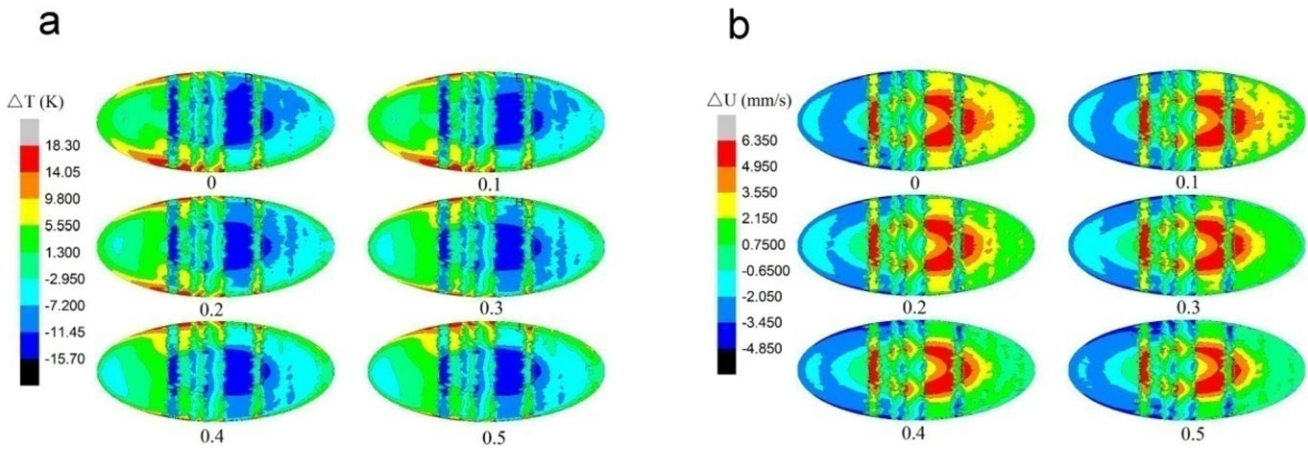

Fig. 2 The vibration mode performance in the central cross section during a half period, (a) temperature and (b) velocity. The velocity amplitude of the vibration source is 0.5 mm/s.

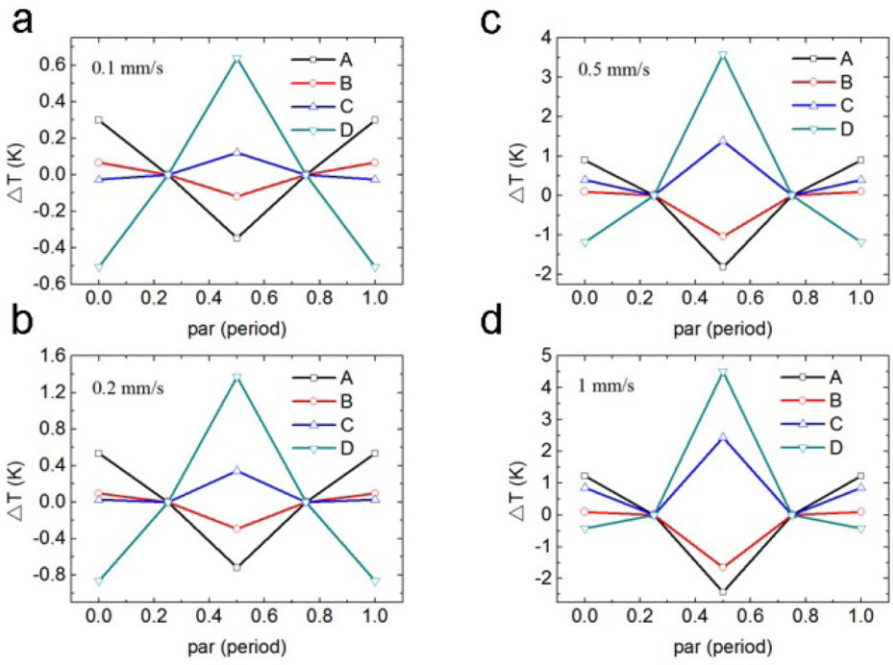

Fig. 3 The vibration mode of temperature for different velocity amplitude of the vibration source at the reference points, (a), (b), (c), (d) are corresponding to the vibration source velocity amplitude of 0.1, 0.2, 0.5, 1 mm/s, respectively.

estimate the sound velocity [23]. The correlative equation is written as follow:

$$\log c = 0.5526 \log(\sigma/\rho) + 5.4364 \tag{11}$$

Where c is the sound velocity, σ is the surface tension, and ρ is the density of melt. Then the estimated sound velocity is 1106.488 m/s. When the vibration propagates from one side to the other side of the crucible wall, it damps due to the viscous dissipation, to the friction of the crucible wall and to energy exchange with the surrounding gas. Thus, the reflection energy of the vibrations is negligibly small. The lifetime of the vibration mode can be estimated as follow,

$$\tau = d/c \tag{12}$$

Where, c is the sound velocity in the melt, and d is the crucible diameter. Then τ is 6.3263 10^{-5} s. Up to now, in the CZ configuration mentioned above, the realistic temperature and velocity fluctuation can be estimated quantitatively according to Eq. (3). (The MATLAB codes

CRYSTAL Research & Technology

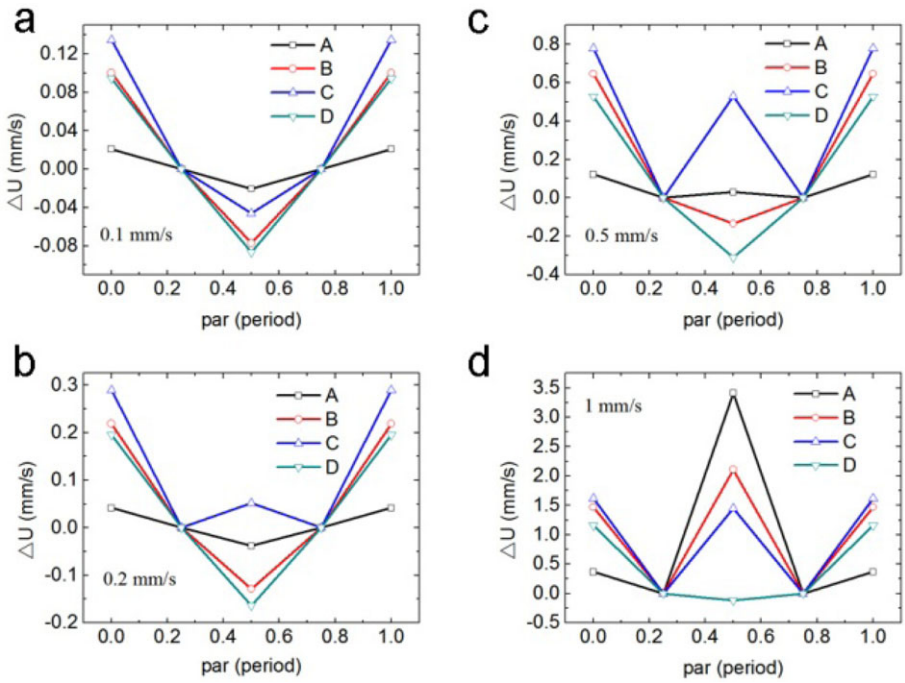

Fig. 4 The vibration mode of velocity for different velocity amplitude of vibration source at the reference points, (a), (b), (c), (d) are corresponding to the vibration source velocity amplitude of 0.1, 0.2, 0.5, 1 mm/s, respectively.

Table 3 The amplitude of the temperature vibration mode.

	A		B		C		D	
	A_1	A_2	A_1	A_2	A_1	A_2	A_1	A_2
Velocity amplitude (mm/s)	(K)							
0.1	0.2988	−0.3477	0.0656	−0.1202	−0.0270	0.1215	−0.5048	0.6400
0.2	0.5319	−0.7201	0.0926	−0.2962	0.0250	0.3401	−0.8640	1.3732
0.5	0.8942	−1.8170	0.1005	−1.0401	0.4006	1.3812	−1.1817	3.5700
1.0	1.2233	−2.4272	0.1013	−1.6560	0.8478	2.4378	−0.4283	4.5023

to compute the realistic transient fluctuation is available in the supplementary.)

4 Results and discussion

The transient fluctuation of temperature is simulated for different crucible vibration amplitude at the reference points. Here, the frequency of the vibration source is 20 kHz. As shown in figure 5, the transient temperature fluctuation intensifies as the velocity amplitude of vibration source increases. The reference point D has the largest fluctuation, C comes second, A and B have smaller fluctuation. The fluctuation of reference points A and B are always positive, that of C and D are always negative. It is caused by the heat flux from the periphery to the center due to the crucible vibration. Reference point C locates in the vicinity of two neighboring crucible wall, the vibration effect is partially offset. So less heat flows from C to B, then the temperature fluctuations at points B and C are smaller.

To get more insights about the transient performance, the transient velocity fluctuation is computed accordingly, as shown in figure 6. The fluctuations at reference points B and D intensify as the velocity amplitude of the vibration source increases. Point A has almost no fluctuation at smaller amplitude, but it unexpectedly increases

Table 4 The amplitude of the velocity vibration mode.

	A		B		C		D	
	A1	A2	A1	A2	A1	A2	A1	A2
Velocity amplitude (mm/s)	(mm/s)							
0.1	0.0208	−0.0205	0.1002	−0.0772	0.1344	−0.0458	0.0944	−0.0866
0.2	0.0417	−0.0383	0.2186	−0.1289	0.2894	0.0514	0.1955	−0.1636
0.5	0.1224	0.0297	0.6465	−0.1343	0.7790	0.5286	0.5285	−0.3115
1.0	0.3655	3.4121	1.4667	2.1082	1.6146	1.4521	1.1525	−0.1221

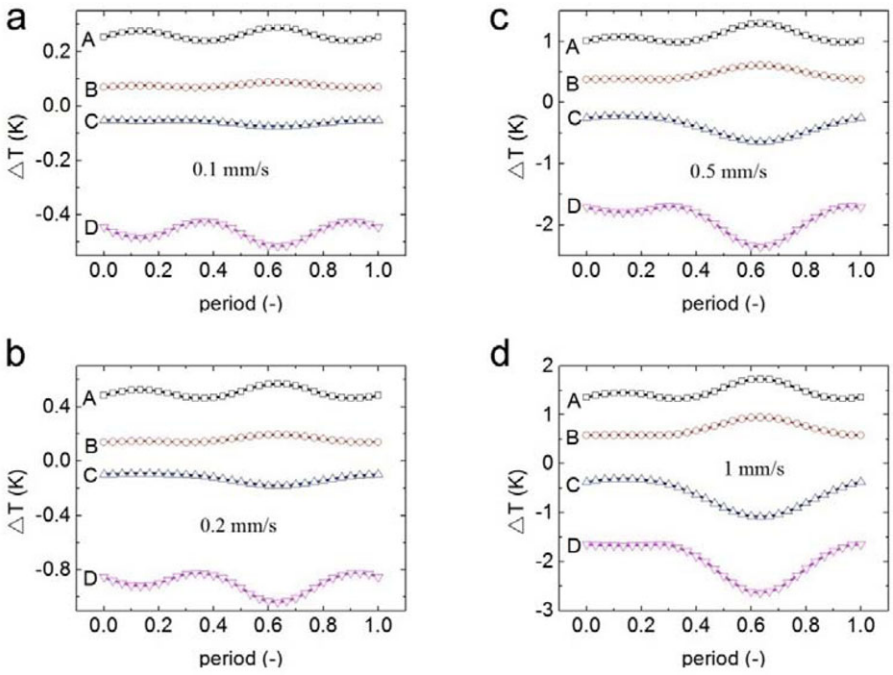

Fig. 5 The transient temperature fluctuation for different vibration source velocity amplitude during one period ($\nu = 20$ kHz), (a), (b), (c), (d) are corresponding to the vibration source velocity amplitude of 0.1, 0.2, 0.5, 1 mm/s, respectively.

to the largest when the amplitude increases to 1 mm/s. It can be explained that point A locates at the center of the crucible, so a smaller asymmetric boundary vibration cannot cause asymmetry fluctuation at the center. The fluctuation at point C is not sensitive to the velocity amplitude of the vibration source. It derives from the offset between two neighboring crucible walls, and is similar to the temperature fluctuation. In the case of 1 mm/s vibration velocity amplitude, points A and B have a negative velocity fluctuation, which reveals a flow from the crucible wall to the central part, then go downwards along the central axis of the crucible.

Figure 7 shows the dependence of the transient temperature fluctuation on the frequency of the vibration source. The temperature fluctuation increases dramatically as the frequency increases. The vibration boundary conditions are asymmetric, which causes asymmetric vibration mode. Thus the fluctuation rate, denoted by $\nu.A\cos(2\pi\nu t)$, of the vibration mode increases accordingly. With the vibration source velocity amplitude of 1 mm/s, the temperature fluctuation varies about 0∼1.6 K for point A, 0 ∼ 1 K for point B, 0 ∼ −1 K for point C and 0 ∼ −2.5 K for point D. The velocity fluctuation is similar to the temperature fluctuation, as shown in

CRYSTAL Research & Technology

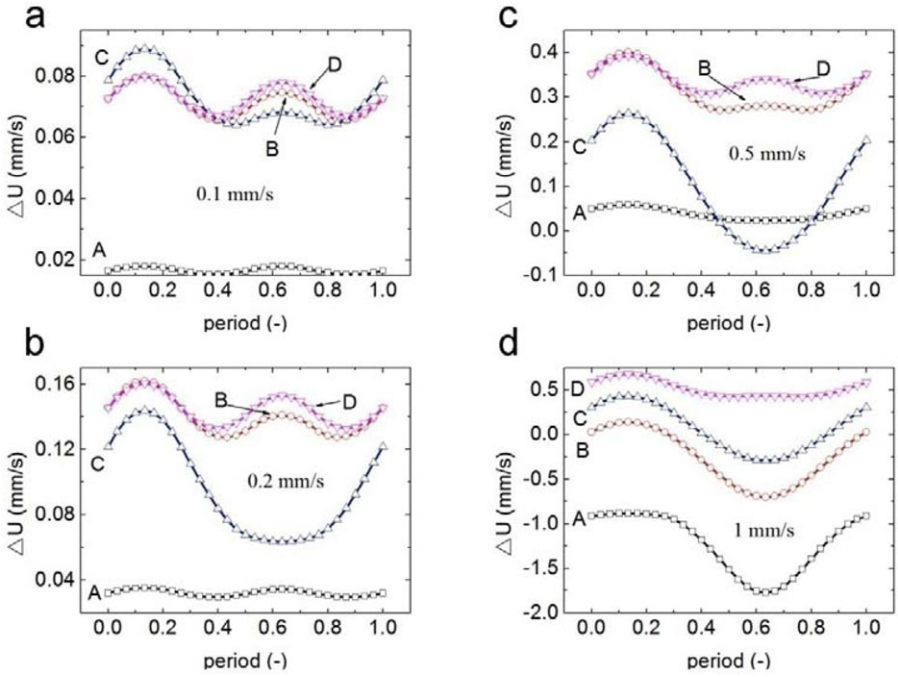

Fig. 6 The transient velocity fluctuation for different vibration source velocity amplitude during one period ($\nu = 20$ kHz), (a), (b), (c), (d) are corresponding to the vibration source velocity amplitude of 0.1, 0.2, 0.5, 1 mm/s, respectively.

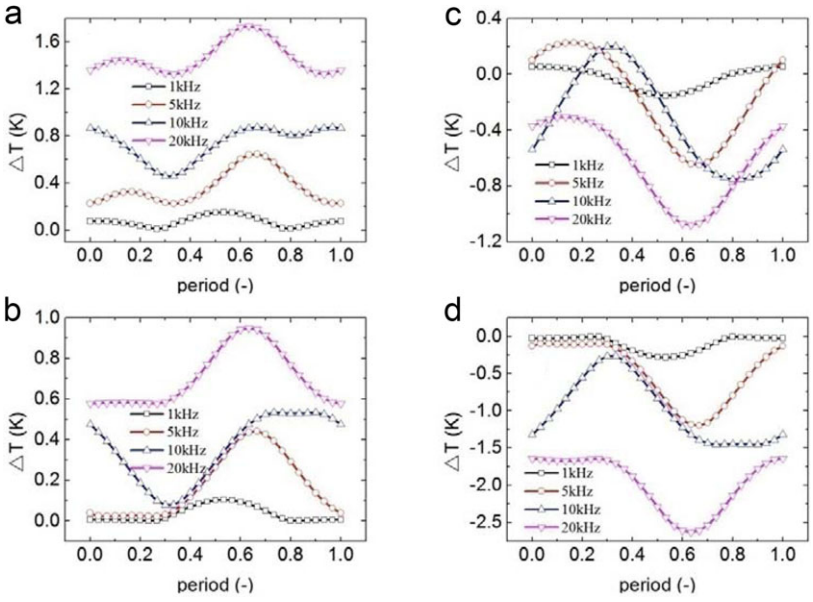

Fig. 7 The transient temperature fluctuation for different frequencies of the vibration source during one period ($A = 1$ mm/s), (a), (b), (c), (d) correspond to different reference points.

figure 8. The waveform corresponds to the cosine boundary conditions is quasi-cosine. From the transient performance of points A and D, we can clearly identify the intensive circuit from the crucible wall to the center at high vibration frequency.

The realistic temperature near point C is measured by submerging a thermocouple under the melt, as shown in figure 1(b). The thermocouple is 's' type with an error range of ±0.1 K. Herein, only the data at the middle stage (which is corresponding to the 3D model geometry in this paper.) of the constant-diameter process is picked up. While the time scale is about 0.1 milliseconds in the realistic situation, it is not accessible for measurement. So we collect the measured temperature values every 3 seconds, and the comparison is qualitative. As mentioned above, the transient

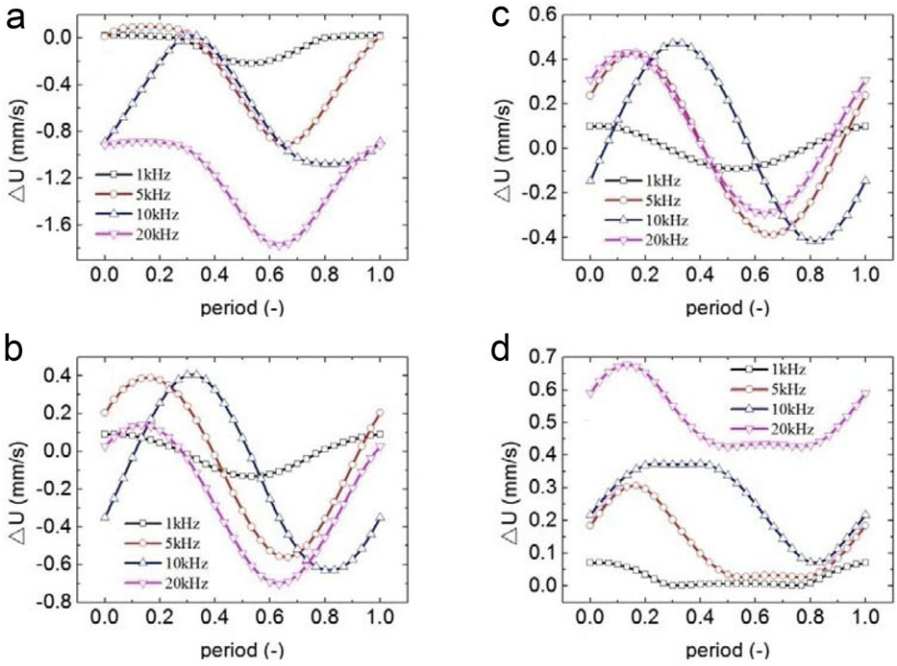

Fig. 8 The transient velocity fluctuation for different frequencies of the vibration source during one period ($A = 1$ mm/s), (a), (b), (c), (d) correspond to different reference points.

temperature fluctuation of the point C is always negative, so the experimental temperature fluctuations are obtained by subtracting the measured maximum with the measured values. The crucible vibration velocity amplitude is uncertain, so a group of velocity amplitudes, *i.e.* 0.1 mm/s, 0.2 mm/s, 0.5 mm/s and 1 mm/s, is compared to the measured results at the experimental electromagnetic field frequency. The results are shown in figure 9. The experiment curve has a similar waveform to the simulation. In the case of 0.3 ∼ 0.4 mm/s or so, the amplitude of the temperature fluctuation excellently agrees with the experimental data. It corroborates our simulation method.

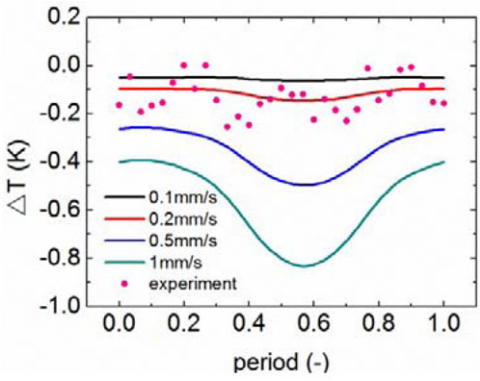

Fig. 9 The measured temperature fluctuations within one minute are compared to the simulated temperature fluctuations at the reference point C. The period related to simulation is 0.05 milliseconds, the experimental data are collected every 3 seconds, so it is a qualitative comparison about the fluctuation amplitude and the waveform.

In the numerical simulation, a non-axisymmetric vibration boundary condition is used, leads to asymmetric vibration modes. As is demonstrated in section 2.1, the realistic transient fluctuation in the melt is a collective effect of the surviving vibration modes. In the case of asymmetric vibration source, as the vibration frequency increases, the fluctuation rate $v.A\cos(2\pi vt)$ increases linearly, then the vibration effect increases. For the axisymmetric vibration source, the vibration mode will be symmetric, *i.e.* it can be formulated with inverse extreme of amplitude. Therefore, if the vibration source is periodic and the lifetime of the vibration mode is an integral multiple of the vibration source period, the collective effects will offset mutually. For some vibration source frequencies, the vibration effect is minimal. Because the realistic data of the vibration mode lifetime is not available, we cannot theoretically estimate these frequencies related to different devices. However, it is feasible to obtain these special frequencies with experiment. In other

CRYSTAL Research & Technology

words, the vibration effect can be enhanced or weakened by the frequency regulation.

5 Conclusions

A general method to study the transient performance of the high frequency vibration in crystal growth is developed. An example during the Czochralski crystal growth has been simulated, and the simulation excellently agrees with the experimental data. Based on the model and the simulation results, the influences of the vibration frequency on the transient fluctuations for temperature and velocity are elucidated. In the case of the asymmetric vibration source, as the vibration frequency increases, the vibration effect increases. For the axisymmetric vibration source, we conclude that at some vibration source frequencies, the vibration effect will be minimal. The vibration effect can be enhanced or weakened by frequency regulation.

Acknowledgement. This work was supported by the National Natural Science Foundation through the funds (11232015, 11072271), and Research Fund for the Doctoral Program of Higher Education of China (20120171110005, 20130171130003).

Key words. computer simulation, crystallization, solidification, growth from melt.

References

[1] M. Asta, C. Beckermann, A. Karma, W. Kurz, R. Napolitano, M. Plapp, and R. Trivedi, Acta. Mater. **57**(4), 941–971 (2009).
[2] W. J. Boettinger, S. R. Coriell, A. L. Greer, A. Karma, W. Kurz, M. Rappaz, and R. Trivedi, Acta. Mater. **48**(1), 43–70 (2000).
[3] E. V. Zharkov, L. V. Prihod'KO, and N. R. Storozhev, Cryst. Res. Technol. **24**, 4761–765 (1989).
[4] I. Ch. Avetissov, A. P. Sadovskii, E. A. Sukhanova, E. V. Zharikov, A. I. Belogorokhov, and B. N. Levonovich, J. Cryst. Growth **312**, 1104 (2010).
[5] G. N. Kozhemyakin, Ultrasonics **54**, 731–736 (2014).
[6] G. N. Kozhemyakin, Ultrasonics **35**, 599–604 (1998).
[7] G. N. Kozhemyakin, J. Cryst. Growth **257**, 237–244 (2003).
[8] H. Nguyen-Thi, Y. Dabo, B. Drevet, M. D. Dupouy, D. Camel, B. Billia, and A. Chilton, J. Cryst. Growth **281**(2), 654–668 (2005).
[9] I. Ch. Avetissov, E. A. Sukhanova, A. P. Sadovskii, V. A. Kostikov, and E. V. Zharikov, J. Cryst. Growth **312**, 1429–1433 (2010).
[10] I. Ch. Avetissov, A. P. Sadovskii, E. A. Sukhanova, and E. V. Zharikov, J. Cryst. Growth **318**, 979 (2011).
[11] I. V. Barmin, A. S. Senchenkov, I. Ch. Avetisov, and E. V. Zharikov, J. Cryst. Growth **275**, 1487 (2005).
[12] Y. Zhang, Y. Liu, W. Jiang, X. H. Pan, W. Q. Jin, and F. Ai, J. Cryst. Growth **310**, 5432 (2008).
[13] H. Nguyen-Thi, G. Reinhart, B. Zhou, B. Billia, Q. Liu, T. P. Lyubimova, and B. Roux, J. Cryst. Growth **275**, 1579–1584 (2005).
[14] G. N. Kozhemyakin, L. V. Zolkina, and Y. Inatomi, Cryst. Growth Des. **6**(10), 2412–2416 (2006).
[15] G. N. Kozhemyakin, J. Cryst. Growth **360**, 35–37 (2012).
[16] I. Ch. Avetissov, A. Sadovskiy, S. Belov, A. Khomyakov, K. Rekunov, V. Kostikov, and E. Sukhanova, Cryst. Eng. Comm. **15**, 2213 (2013).
[17] I. Ch. Avetissov, A. P. Sadovskiy, E. A. Sukhanova, G. Yu. Orlova, I. A. Belogorokhov, and E. V. Zharikov, J. Cryst. Growth **360**, 167–171 (2012).
[18] K. S. Holian, T-4 Handbook of Material Properties Data Bases (Los Alamos National Laboratory, 1984).
[19] T. Tsukada, M. Hozawa, and N. Imaishi, J. Chem. Eng. Japan **27**, 25–31 (1994).
[20] C. J. Jing, T. Tsukada, M. Hozawa, K. Shimamura, N. Ichinose, and T. Shishido, J. Cryst. Growth **265**, 505–517 (2004).
[21] C. W. Lan, Chem. Eng. Sci. **59**(7), 1437–1457 (2004).
[22] X. L. Li, Y. L. Liu, B. Wang, and Y. Z. Zhu, Cryst. Res. Technol. 1–7 (2014). DOI:10.1002/crat.201400014.
[23] S. Blairs, J. Colloid. Interf. Sci. **302**, 312–314 (2006).